Chinese Journal of Structural Chemistry

REVIEW

Soft X-Ray Absorption Spectroscopy of Advanced Two-Dimensional Photo/Electrocatalysts for Water Splitting

Xiaoxin Lv[1], Guoqing Li[1], Gaoteng Zhang[2], Kun Feng[2], Jiujun Deng[1]* and Jun Zhong[2]*

[1]*Institute for Energy Research, Automotive Engineering Research Institute, Jiangsu University, Zhenjiang 212013, China*

[2]*Institute of Functional Nano and Soft Materials Laboratory (FUNSOM), Jiangsu Key Laboratory for Carbon-Based Functional Materials & Devices, Soochow University, Suzhou 215123, China*

ABSTRACT Photo/electrocatalytic water splitting has been considered as one of the most promising approaches for the clean hydrogen production. Among various photo/electrocatalysts, 2D nanomaterials exhibit great potential because of their conspicuous properties. Meanwhile, synchrotron-based soft X-ray absorption spectroscopy (XAS) as a powerful and element-specific technique has been widely used to explore the electronic structure of 2D photo/electrocatalysts to comprehensively understand their working mechanism for the development of high-performance catalysts. In this work, the recent developments of soft XAS techniques applied in 2D photo/electrocatalysts have been reviewed, mainly focusing on identifying the surface active sites, elucidating the location of heteroatoms, and unraveling the interfacial interaction in the composite. The challenges and outlook in this research field have also been emphasized. The present review provides an in-depth understanding on how soft XAS techniques unravel the correlations between structure and performance in 2D photo/electrocatalysts, which could guide the rational design of highly efficient catalysts for photo/electrocatalytic water splitting.

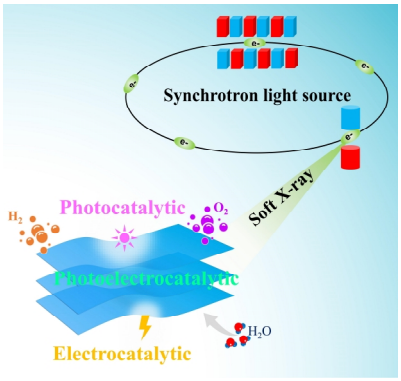

Keywords: two-dimensional materials, photocatalyst, electrocatalyst, water splitting, soft XAS

n INTRODUNTION

As a clean energy source, hydrogen has been recognized as a promising alternative to fossil fuels for a low-carbon society. However, the present hydrogen production is mostly via the steam reforming of natural gas, which not only aggravates the consumption of fossil fuels but also gives rise to global warming via the massive emission of CO_2. Within this context, the development of sustainable technologies for the clean hydrogen yield has attracted significant attentions.[1] Particularly, the photo/electrocatalytic (photocatalytic, electrocatalytic, and photoelectrocatalytic) water splitting from the renewable energy sources has been considered as the most viable approach.[2-4] As shown in Figure 1a, the photocatalytic water splitting reaction usually involves three steps: light absorption over photocatalysts to generate the hole/electron pairs (step 1), photoexcited carrier separation and migration (step 2), and surface redox reaction for the oxygen and hydrogen evolutions (step 3).[3] Through this reaction, hydrogen can be produced from abundant solar energy and water with low-cost and environment-friendly features. Different from the photocatalytic water splitting in which the reaction is driven by solar energy, the electrocatalytic water splitting reaction is commonly proceeded by electric power with more facilitated charge separation and transfer for a higher hydrogen yield.[4] As displayed in Figure 1b, the electrocatalytic water splitting contains two independent half-reactions: hydrogen evolution reaction (HER) on the cathode and oxygen evolution reaction (OER) on the anode. Furthermore, by integrating the merits of photocatalytic and electrocatalytic water splitting, photoelectrocatalytic water splitting inherits the accelerated charge dynamics and meanwhile reduces the consumption of electrical power, consequently offering an intermediate hydrogen production efficiency at an affordable cost.[2] As shown in Figure 1c, photoelectrocatalytic water splitting reaction is generally driven by the sunlight and the external bias, and after the three steps similar to those for photocatalytic water splitting, the oxygen is generated at the surface of photoanode while the hydrogen is evolved at the surface of photocathode. Despite there are distinct differences in the working mechanisms and the devices of these three systems, the rational design of high-performance photo/electrocatalysts is a common and critical issue towards the efficient water splitting. In such cases, the development of photo/electrocatalysts with high efficiency, superior stability, and low cost has been the focus of a

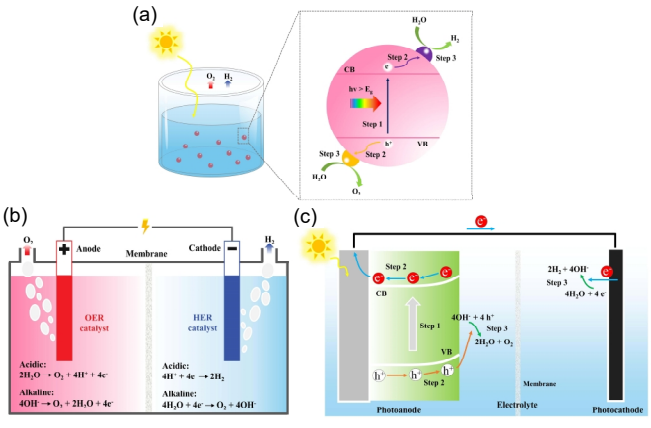

Figure 1. Schematic illustration of (a) photocatalytic, (b) electrocatalytic, and (c) photoelectrocatalytic water splitting.

DOI: 10.14102/j.cnki.0254-5861.2022-0099

Chinese Journal of Structural Chemistry

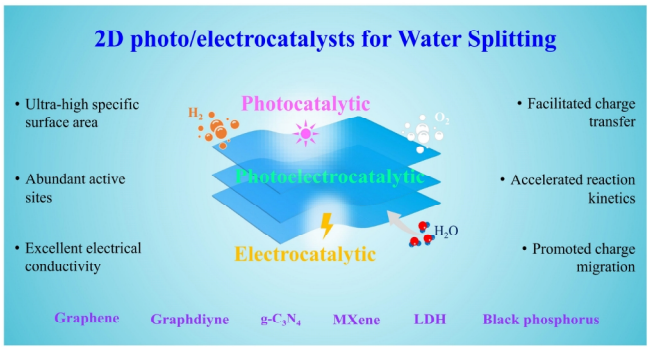

Figure 2. Distinct properties and applications of 2D photo/electrocatalysts.

wide variety of research.[2-4]

Until now, numerous advanced materials including noble metals,[5] transition metal-based compounds,[6,7] single atoms,[8] high-entropy alloys,[9] organic semiconductors,[10] and two-dimensional (2D) nanomaterials[11-15] have been widely explored as the photo/electrocatalysts for water splitting. Among them, 2D nanomaterials hold great potential on account of their unique and outstanding characteristics, such as large reactive surface area, abundant active sites, excellent electrical conductivity, and tunable energy structure,[11-15] which can significantly facilitate the charge diffusion and accelerate the kinetic for water splitting. As demonstrated in Figure 2, the structure-activity relationship in 2D photo/electrocatalysts can be briefly illustrated as follows:

(1) Ultra-high specific surface area for the facilitated charge transfer. In comparison to other nanosized materials such as 0 D nanodots, 1D nanowires, 3D nanoballs, and their bulk counterparts, the atomically thin configuration of 2D nanomaterials endows a large specific surface area, which can remarkably shorten the charge migration distance from the generated location to the surface active sites, and simultaneously facilitate the charge transfer across the interface by increasing the contact area between catalysts and reactant.[11-15] Taking single-layered graphene as an example, the considerable theoretical specific surface area of >2600 m^2 g^{-1} is highly favorable for the photo/electrocatalytic water splitting reaction by acting as a promising support/substrate.[16]

(2) Abundant surface active sites for the accelerated water splitting reaction. The geometric configurations of 2D nanomaterials not only guarantee the large surface area but also expose plenty of unsaturated surface dangling atoms, which as the active sites are of significance for the adsorption of water molecule and intermediates, as well as the desorption of H_2 and O_2 molecules.[17] Moreover, for the composite photo/electrocatalysts, abundant active sites of 2D nanomaterials can strongly bind the confined material, hence reducing the interfacial charge transfer barrier for constructing a more efficient composite.[18] For example, black phosphorus (BP) exhibits abundant active sites from uncoordinated lone pair electrons of P atom and unavoidable point defects, which endows it an inborn and superior photo/electrocatalytic activity.[19]

(3) Excellent electrical conductivity for the promoted charge migration. High electrical conductivity has been widely reported for various 2D nanomaterials such as graphene, black phosphorus (BP), as well as metal carbides and nitrides (MXenes).[20] Taking the case of Ti_3C_2 MXene, its electrical conductivity is as high as 2.4 × 10^4 S cm^{-1}.[21] Upon using as photo/electrocatalysts, the superior electrical conductivity will be definitely beneficial for reducing the charge migration resistance, and consequently lead to a faster charge transport during the water splitting reaction.

2D nanomaterials also possess other conspicuous advantages such as tunable band gap for the enhanced light absorption and prominent mechanical properties for the high catalytic durability.[16,20] On account of these superiorities, 2D nanomaterials have been widely employed in the field of photo/electrocatalytic water splitting with great progresses achieved in the past decades.

Nevertheless, the lack of a knowledge of reaction mechanisms at atomic level still retards the rational design of highly active 2D photo/electrocatalysts.[11-15] On one side, surface active sites have been demonstrated to be positively associated with the catalytic performance. However, the complicated processes in photo/electrocatalytic water splitting make the accurate identification of active sites nearly impossible. In especial, for 2D photo/electrocatalysts, abundant unsaturated surface atoms can be observed and any of them can probably be utilized as the real active sites to drive the water splitting reaction.[22,23] On the other side, the development of efficient strategies to boost the photo/electrocatalytic activities of 2D nanomaterials has been the major subjects of interests.[24-28] Particularly, the heteroatom doping and composite construction have been found to be the most effective routes by increasing the amounts of active sites and integrating the benefits of each component, respectively.[26-28] Whilst, the utilization of conventional characterization tools to elucidate the exact location of heteroatoms and unveil the interfacial component interaction is still a great challenge.[22,29] As a result, it is essential to develop advanced and more powerful techniques to further understand the fundamental working mechanisms of 2D photo/electrocatalysts for water splitting.

Among various advanced characterization techniques, synchrotron-based X-ray absorption spectroscopy (XAS) stands out as an element-specific method to acquire the chemical states, electronic structures, and local coordination environments of materials.[30-35] In especial, the applications of XAS in the soft X-ray range (soft XAS) have received increasing interests since it is powerful in clarifying the electronic structure of species with tunable detection depth.[31,33-35] In the meantime, it is well known that the photo/electrocatalytic water splitting reaction generally takes place on the surface or near surface layers of catalysts.[36,37] Therefore, through soft XAS measurements, the inactive and active sites of 2D photo/electrocatalysts can be clearly distinguished, with the detection of heteroatoms' location and the identification of interfacial interaction between different components. For instance, through N and C K-edge XAS studies for Ni single atoms decorated carbon nanosheets, Li et al. demonstrated the successful Ni functionalization on the carbon support via forming Ni-N bonding.[38] Moreover, by conducting B and O K-edge XAS measurements for oxygen doped hexagonal boron nitride (h-BN) nanosheets, the incorporation of O atoms into the

DOI: 10.14102/j.cnki.0254-5861.2022-0099

h-BN lattice at the original N position has also been clearly revealed.[39] Such studies have sprung up in recent years. Meanwhile systematic reviews summarizing the progress achieved in synchrotron-based XAS for (photo)electrocatalytic water splitting have also been widely reported.[40,41] However, a comprehensive overview on the application of soft XAS in 2D photo/electrocatalyst-based water splitting is still rare. Within this regard, this review starts with a brief description of soft XAS technique, followed by a highlight of recent studies of soft XAS characterizations for 2D photo/electrocatalysts, particularly for the identification of active sites, the clarification of heteroatom location, and the unraveling of interfacial interaction between different components. Additionally, soft XAS for 2D nanomaterial-based photoelectrocatalytic water splitting has also been emphasized in this section. Finally, it ends with a summary of current challenges and outlook for future research. This review will provide more guides for the fabrication of highly-active 2D photo/electrocatalysts, and meanwhile promote the utilization of soft XAS techniques in the field of photo/electrocatalytic water splitting.

n POWERFUL FEATURES OF SOFT XAS FOR 2D PHOTO/ELECTROCATALYSTS

Due to the prominent advantages of synchrotron X-rays, such as high brightness, tunable energy, and partial coherence, synchrotron-based X-ray absorption spectroscopy (XAS) as a powerful and element-specific tool has been widely utilized to explore the local geometric and electronic structures of matters.[30-35] This technique yields the element- and symmetry-specific information of the unoccupied states by measuring the X-ray absorption coefficient of a material as a function of the photon energy,[42] as shown in Figure 3. More notably, owing to the direct exploration of the transitions between atomic energy levels, XAS can provide more useful information with atomic precision compared with conventional chemical state analysis techniques, such as X-ray photoelectron spectroscopy (XPS) and electron energy loss spectroscopy (EELS).[35]

Generally, based on the photon energy of X-ray, XAS can be classified into soft XAS (< 2 keV) and hard XAS (> 4 keV).[34,35,42]

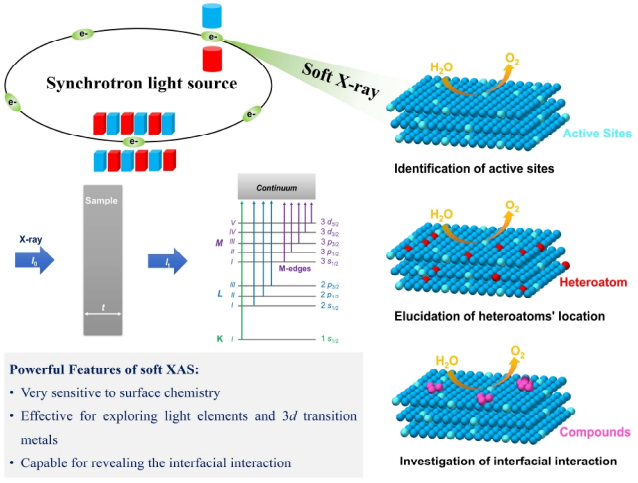

Figure 3. Applications of soft XAS for 2D photo/electrocatalysts.

Meanwhile, an XAS spectrum can also be divided into two regions: X-ray absorption near-edge structure (XANES, from the absorption edge to 50 eV above the edge) and extended X-ray absorption fine structure (EXAFS, from 50 eV above the edge to as high as 1000 eV).[34,42] In the field of soft XAS, XANES is typically measured, which endows an insight into the chemical state of absorption atom by acquiring its oxidation state and strength of chemical bonding with the nearest neighbors and the electronic structure of unoccupied molecular orbitals or bands.[33-35] This clearly indicates that in many ways, soft XAS is superior to conventional characterization tools for the structure-property relationship in 2D photo/electrocatalysts, as described in Figure 3 and as follows:

(1) The energy range of soft XAS is very suitable to investigate the local structure of various elements, such as K-edge of B, C, N, O, and L-edge of S and P, as well as L-edge of 3*d* transition metals such as Fe, Co, Ni, Ti, Mo, and Mn.[42,43] Most of these elements are involved in typical 2D photo/electrocatalysts, for example, graphene, graphdiyne, graphitic carbon nitride (g-C_3N_4), layered double hydroxide (LDH) nanosheets, MXenes, black phosphorus (BP), boron nitride (h-BN), as well as 2D metal organic frameworks (MOF). Consequently, soft XAS is highly productive to elucidate the electronic structure and bonding information of 2D photo/electrocatalysts at atomic level.

(2) Due to the disparate probing depth of hard and soft X-ray (e.g., for 3d transition metals, this is a few nanometers for soft XAS with total electron yield mode but a few micrometers for hard XAS with transmission mode), soft XAS is very sensitive to explore the surface chemistry of a sample.[34,35] In the meantime, for the photo/electrocatalytic water splitting, surface or near-surface layer has been demonstrated to be where the reaction takes place. As a result, soft XAS is highly effective to unravel the working mechanism of 2D photo/electrocatalysts by identifying their real active sites.

(3) Soft XAS is very useful to separate the spectra features generated by different atoms or by the same atomic element but in different chemical environments.[33,34] That is to say, the chemical bonds and local bonding of a sample can be clearly revealed through the "fingerprint" evidence of soft XAS. A perfect example is the identification of a heterostructure of graphitic carbon ring (C_{ring}) incorporated g-C_3N_4, in which the C K-edge XAS spectrum of heterostructure exhibits an obvious broad peak originated from the formation of sp^2 π-conjugated heterointerface. For comparison, in C 1s XPS the electronic structural alters of C_{ring} incorporated g-C_3N_4 can be acquired but it is hard to accurately identify the location of C_{ring}.[44]

On the other hand, we also note that soft XAS mainly provides qualitative analysis of electronic structures of matters based on the energy position shift, the peak intensity change, or the spectral shape difference. Typically, the quantitative analysis such as EXAFS fitting in hard XAS will not be performed in soft XAS due to the short energy range. Therefore, this review mainly discusses the qualitative ability of soft XAS applied in 2D photo/electrocatalysts.

n SOFT XAS APPLIED IN 2D PHOTO/ELECTROCATALYSTS

DOI: 10.14102/j.cnki.0254-5861.2022-0099

Identifying the Surface Active Sites. As described above, surface active sites have been demonstrated to be very critical for the performance of 2D photo/electrocatalysts by modulating the adsorption and activation of water molecule during the water splitting reaction.[20,23] As a result, clearly identifying the active sites of 2D photo/electrocatalysts will be highly beneficial for unraveling their working mechanisms in more detail. In this regard, soft XAS shows great potential over traditional characterizations owing to its sensitivity to the surface active sites of a sample.

Ni-Fe electrocatalysts as one class of typical earth-abundant transition metal-based compounds have been proven to be the most active OER catalysts.[45,46] However, the detailed role of Ni and Fe sites for the excellent activity is still under debate, and which one is the actual active site is also unclear.[47,48] One opinion is that the outstanding OER performance of Ni-Fe electrocatalysts can be attributed to Ni sites alone because that Ni-based compounds commonly have more excellent catalytic activity than Fe-based electrocatalysts.[49] While, another view suggests that the case of Fe atoms as the reactive sites should also be taken into consideration, because some Fe species in high valence states (e.g., Fe^{IV}) have been found to be very favorable for the accelerated OER kinetics.[50,51] In such cases, despite that numerous studies have demonstrated that the incorporation of Fe into Ni-based compounds could significantly improve their electrocatalytic activities, it is still hard to identify whether Fe would be the active site or not due to the lack of efficient Fe-based OER electrocatalyst. Thus, fabricating efficient electrocatalysts with highly active Fe sites to deeply understand the role of Fe atoms played in the water oxidation process can provide insights into this debate, and will further promote the design of efficient Ni-Fe electrocatalysts. In this regard, Chen et al. took the ultrathin Fe_7S_8 nanosheet as an example and performed Fe L-edge XAS experiments to investigate the detailed electronic structure of active Fe sites.[52] As shown in Figure 4a, the Fe_7S_8 nanosheets exhibited a higher shoulder peak of t_{2g} than that of Fe_7S_8 bulk, suggesting a higher density of t_{2g} unoccupied states in Fe_7S_8 nanosheets originating from the improved electron delocalization. Moreover, the Fe L-edge XAS spectra of Fe_7S_8 nanosheets after the reaction at 1.52, 1.62, and 1.72 V (vs. RHE) were also collected. As depicted in Figure 4b, the intensity of shoulder peak of t_{2g} was gradually increased with the increase of applied bias, indicating the rising t_{2g} unoccupied states in the OER process. Generally, the enhanced unoccupied states can be attributed to the electron loss in the catalysts, i.e., the metal atoms tend to be in high valence states. Therefore, the enhanced t_{2g} unoccupied states strongly suggest that during the OER processes, the Fe atoms in ultrathin Fe_7S_8 nanosheets were mainly in the high valence states, which could act as the reactive sites to greatly facilitate the electron transfer (Figure 4c). This finding provided an insight into the role of Fe atoms played in the OER process, and offered an instructor for the design of efficient Fe-based electrocatalysts.

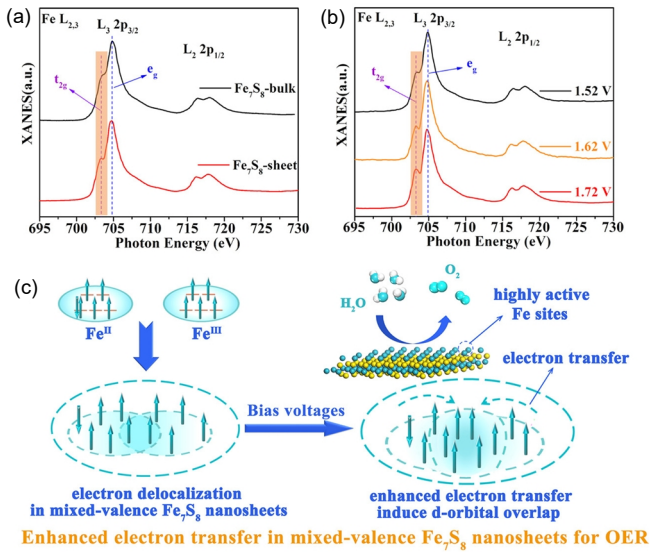

Figure 4. (a) Fe L-edge XAS spectra of Fe_7S_8 nanosheets and bulk sample. (b) Fe L-edge XAS spectra of Fe_7S_8 nanosheets collected at different bias voltages. (c) Schematic illustration for the formation of highly active Fe sites in the mixed-valence Fe_7S_8 nanosheets. Reproduced with permission from Ref. [52].

Recently, transition metal layered double hydroxides (LDHs) as an attractive platform for OER have also been widely reported.[53,54] Especially, the monolayer LDHs have attracted tremendous interests because they possess an additional degree of freedom to adjust the electronic structures and catalytic activities.[55,56] In this regard, Kang et al. developed a facile synthesis of Co-doped $Ni(OH)_2$ (CoNi-LDH) monolayers by an in-situ electrochemical conversion method.[56] Furthermore, by preforming operando Ni, Co, and O K-edge XAS characterizations, an intriguing valence oscillation of Ni and Co atoms with increasing potential was observed. In that study, the Ni K-edge spectrum of CoNi-LDH monolayers before OER measurement presents a spectral shape similar to those of Ni^{2+} in previous studies,[57,58] indicating that the Ni atoms in CoNi-LDH monolayers mainly exist as Ni^{2+}. In the meantime, for the O K-edge XAS spectra collected at different external potentials, sharp pre-peaks (labelled as peak A) from the hybridization of Ni 3d and O 2p orbitals with e_g symmetry and the d_7 (Ni^{3+}) electron configuration were observed. Moreover, it has been found that the intensity of peak A obviously increased after the measurement at 1.30 V. It is well known that the pre-peak intensity presents the density of unoccupied states, thus the increased peak A at 1.30 V was indicative for more unoccupied states and the loss of electrons from Ni (i.e., higher oxidation state of nickel than Ni^{2+}). However, with the increase of potential to 1.35 V, the intensity of peak A suddenly descended, meaning the return of electrons to Ni (decreased oxidation state of nickel) which could be assigned to the generation of oxygen vacancies. Furthermore, when the potential increased to 1.40 V and 1.45 V, the peak A recovered to high intensity as that at 1.30 V, confirming the variations of oxygen vacancies. Overall, the O K-edge XAS data clearly revealed that during the OER process, the valence state of Ni in the CoNi-LDH monolayers showed an obvious oscillation. According to electrochemical results, the increase in the Ni valence state could be attributed to dehydrogenation while the decrease was assigned to deoxygenation with

Chin. J. Struct. Chem. **2022**, 41, 2210016-2210028
DOI: 10.14102/j.cnki.0254-5861.2022-0099

the in-situ generation of oxygen vacancies. The generated oxygen vacancies as the active sites effectively facilitated the OER process, eventually leading to a superior activity.

Soft XAS technique has also been used to identify the active sites in graphene with doping elements.[59-61] Recently, Yang et al. reported the exploration of N-doped graphene nanoribbons with interconnected three-dimensional architecture (labeled as N-GRW) for high-efficient OER and oxygen reduction reaction (ORR).[61] Through the O and N K-edge XAS measurements for N-GRW catalysts before/after ORR and OER treatments, different active sites for OER and ORR processes were identified. As presented in C K-edge XAS spectra in Figure 5a, after OER and ORR experiments, an increased intensity for peak D (287.7 eV) related to $\pi^*_{C\text{-}O\text{-}C,\ C\text{-}N}$ was observed, suggesting the adsorption of intermediate species (O*) on carbon atoms during ORR and OER processes. This conclusion was further confirmed by the formation of a new peak at 289.6 eV after ORR and OER, originating from the adsorption of OOH* intermediates. Figure 5b displayed the N K-edge XAS spectra of N-GRW before and after ORR and OER. There was a new peak at the lower energy side (~401 eV) of graphitic N in the spectrum after ORR, which could be attributed to the distortion of heterocycles caused by the adsorbed O* and OOH* intermediates on carbon atoms near the graphitic N. Meanwhile, the peak at 398.0 eV related to pyridinic N kept unchanged after ORR treatment (Figure 5b). The results suggested that the quaternary N with n-type doping instead of the p-type doping by pyridinic N was the actual active sites for ORR process (Figure 5c). Different from that for ORR treatment, after OER experiments, the full width at half maximum of the pyridinic N peak at ~398.0 eV increased from 0.8 to 1.15 eV accompanied by the generation of a new peak at the higher energy side, as shown in Figure 5b. While, the graphitic and pyrrolic N peaks were similar to those of the pristine N-GRW, indicating the adsorption of OOH* and O* intermediates on carbon atoms next to the pyridinic N during OER process. It suggested that the pyridinic N with p-type doping acted as the active sites for OER (Figure 5c). This result offered more insights for fabricating the high-efficient graphene-based photo/electrocatalysts.

Elucidating the Location of Heteroatoms. Unlike 2D transition metal-based semiconductors which possess inborn catalytic activities and can be directly used as photo/electrocatalysts, some kinds of 2D nanomaterials such as graphene and graphdiyne generally lack intrinsic and sufficient active sites, i.e., they are electrochemically inert toward photo/electrocatalytic water splitting.[16,19] Meanwhile, for some 2D photocatalysts such as g-C_3N_4, their poor charge separation and transport capabilities have turned out to be fatal for the photocatalytic water splitting performance.[62,63] In such cases, different strategies involving element doping, co-catalyst deposition, and composite construction have been developed to overcome the problems, in which the heteroatom incorporation has been demonstrated to be one of the most effective routes by engineering the electronic structures of 2D photo/electrocatalysts.[62-65] Also, soft XAS has been intensively utilized to illustrate the structure-activity relationship in heteroatom incorporated 2D photo/electrocatalysts by elucidating the location and the role of alien atoms.

Graphdiyne (GDY) as a novel carbon allotrope with large π conjugated network has received numerous attentions since the pioneer work in 2010.[66] The substitution of C atoms with alien atoms, such as B, N, and S, to modulate the electronic structures of GDY has also been found to be very effective to greatly improve its electrocatalytic activity.[65,67-69] For instance, Zhao et al. reported that owing to the synergistic effect on faster charge kinetics, the N and S co-doped GDY electrocatalyst showed an higher OER activity than those of N or S separately doped samples.[68] In that work, N and S K-edge XAS measurements were utilized to demonstrate the successful doping of N and S atoms with the identification of their locations. The XAS results clearly demonstrated a new form of nitrogen atoms, i.e., the sp-hybridized nitrogen (sp-N) site was incorporated into GDY, which was found to be associated with the lowered overpotential for OER process. For the subsequent S doping, the sulfur atoms substituted the carbon atoms in benzene ring, which could remarkably improve the current density by facilitating the OER kinetics. This work showed an interesting investigation on the synergistic effects of dual heteroatoms, which might guide the synthesis of high-efficient GDY-based electrocatalysts.

Similar to GDY, transition metal oxides and their derivatives have also been explored as attractive electrocatalysts for water splitting.[6,25] Particularly, cobalt-based oxides have been proven to be one kind of potential OER electrocatalysts, however, their catalytic activities are still severely restricted by slow surface species adsorption and poor carrier transfer.[70,71] In this regard, heteroatom doping is extensively used to overcome these problems. For example, Huang et al. demonstrated that the incorporation of Mn^{4+} dopants into cobalt oxyhydroxide (CoOOH) nanosheets could greatly enhance the OER activity by facilitating the proton-electron transfer kinetics and simultaneously decreasing

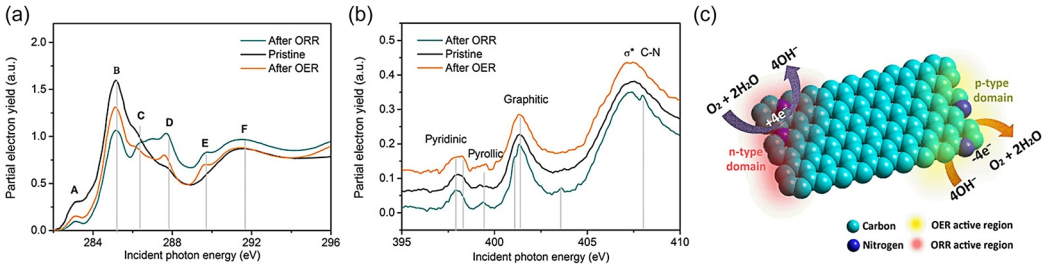

Figure 5. (a) C K-edge and (b) N K-edge XAS spectra of N-GRW catalysts, pristine (black line), after ORR (yellow line) and after OER (blue line). (c) Schematic diagram of ORR and OER occurring at different active sites on the n- and p-type domains of the N-GRW catalysts. Reproduced with permission from Ref. [61].

DOI: 10.14102/j.cnki.0254-5861.2022-0099

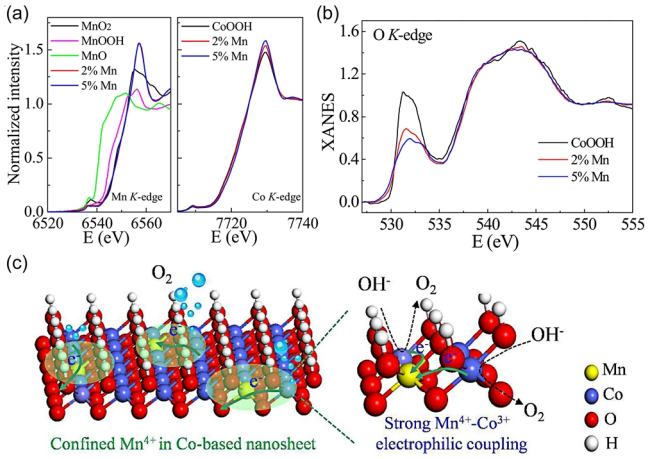

Figure 6. (a) Mn K-edge (left), Co K-edge (right) and (b) O K-edge XAS spectra of Mn doped CoOOH nanosheets. (c) Schematic illustration of working mechanism for Mn doped CoOOH nanosheets. Reproduced with permission from Ref. [72].

the charge transport resistance.[72] To clarify how the Mn incorporation altered the electronic structure of CoOOH nanosheets, the Mn, Co, and O K-edge XAS measurements for Mn-doped CoOOH were performed. Figure 6a illustrates the Mn K-edge XAS of Mn doped CoOOH nanosheets with MnO, MnO_2, and MnOOH as the references. Clearly, the Mn doped CoOOH nanosheets exhibited similar absorption edge to that of MnO_2 but different from those for MnOOH and MnO, indicating that the Mn dopants in Mn doped CoOOH nanosheets are mainly Mn^{4+}. Figure 6b shows the O K-edge XAS spectra of as-obtained samples, in which three characteristic peaks were obviously observed. It is noted that in comparison of pure CoOOH, the first peak (originated from the transition from O 2p to hybridized unoccupied Co e_g states[73]) for Mn doped CoOOH nanosheets was broadened and the corresponding intensity also declined with the increase of Mn concentration, suggesting that the unoccupied Co e_g states of Mn doped CoOOH are lower than that of pure CoOOH. This phenomenon could be assigned to the electron extraction of Co $3d^6$ orbital caused by Mn^{4+} incorporation, which led to the redistribution of Co 3d electronic configuration with more occupied e_g states. Subsequently, electrochemical measurements further revealed that this optimized d-orbital configuration could remarkably promote the Co oxidization ability (Figure 6c) and lead to an enhanced OER activity.

Heteroatoms' incorporation has also been used to boost the photocatalytic performance of g-C_3N_4 by improving its sunlight harvesting and/or accelerating the charge transfer.[62,64] Zhao et al. reported the synthesis of B dopant and N defect co-incorporated g-C_3N_4 via calcining the mixture of g-C_3N_4 and $NaBH_4$ in an inert atmosphere (Figure 7a).[74] Notably, on account of the enhanced optical absorption in visible light and the facilitated charge transfer, the as-obtained sample exhibited an excellent photocatalytic oxygen evolution activity. Furthermore, to elucidate the co-incorporation of B dopants and N defects into g-C_3N_4, N and C K-edge XAS characterizations for the pristine g-C_3N_4, B doped sample (CN-B), N defect incorporated sample (CN-H), and B dopant and N defect co-treated sample at 400 °C (BH-400) were performed to explore the electronic structure evolution. As displayed in Figure 7b, the N K-edge XAS spectra of all samples showed two distinct 2p π^* resonances at about 400.3 and 403.3 eV, which could be attributed to triangular edge N (N1 site) and bridge N (N2 site) of g-C_3N_4, respectively.[75,76] Figure 7b also depicts that the peak intensity ratio of N1/N2 in CN-B sample is nearly the same as that of pristine g-C_3N_4, indicating the ratios of N atoms at N1 and N2 sites in both samples are similar. It further implied that in CN-B sample, no N defects were introduced while B dopants were located at the carbon sites. Moreover, compared with that of pristine g-C_3N_4, CN-B sample exhibited a decreased intensity for N K-edge XAS, which could be assigned to the electron back-donation from B to N site, given the electronegativity of B is lower than those of C and N. Similar declined intensity of N K-edge XAS could also be observed in CN-H sample due to the formation of nitrogen defects in CN-H.[77] More notably, the peak intensity ratio of N1/N2 in CN-H (≈1.3) is larger than that of pristine g-C_3N_4 (≈1.2), suggesting more defects at N2 sites in CN-H sample. Furthermore, for BH400 sample, it is clearly seen that both N1 and N2 peaks are less intense than that in CN-B or CN-H, indicating the co-existence of electron back-donation effect and nitrogen defects in BH400 sample.

Figure 7c shows the C K-edge XAS spectra of the pristine g-C_3N_4, CN-B, CN-H, and BH-400 samples, in which two major peaks at about 285.5 eV (peak C_a) and 288.4 eV (peak C_b) are clearly found. Peak C_a could be ascribed to the defect structure in g-C_3N_4 framework.[75] As presented in the inset of Figure 7c, the CN-B, CN-H, and BH400 samples exhibited larger area and higher intensity of peak C_a than that of the pristine g-C_3N_4, suggesting more defective structure in doped samples. While for

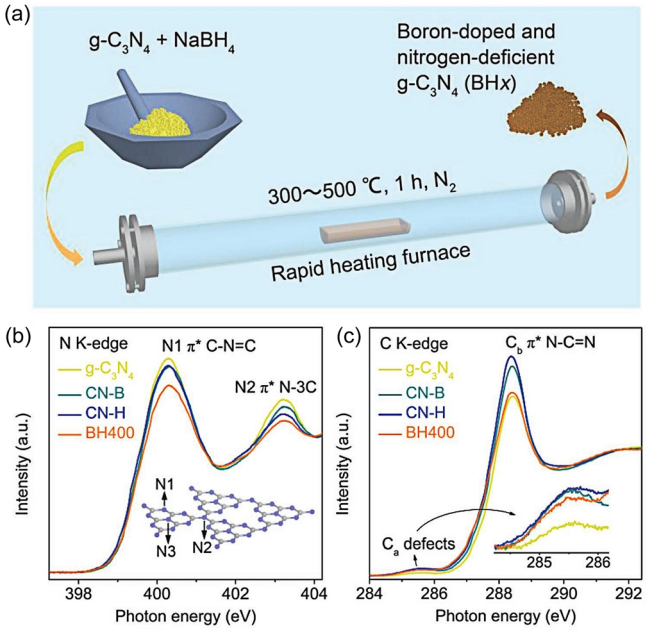

Figure 7. (a) Schematic illustration of the preparation process of $NaBH_4$ treated g-C_3N_4 samples. (b) N K-edge and (c) C K-edge XAS spectra of different samples. Reproduced with permission from Ref. [74].

Chin. J. Struct. Chem. **2022**, 41, 2210016-2210028
DOI: 10.14102/j.cnki.0254-5861.2022-0099

peak C_b, it is attributed to the electron transition from the C 1s to 2p π^* orbital related to N-C=N sp^2 hybridized states.[78] The declined intensity of peak C_b generally indicated the poor crystallinity or disordered atomic environment.[77] Based on these reports, lower intensity of peak C_b in BH400 sample signified more disordered structures, as shown in Figure 7c. To sum up, all these XAS results clearly revealed that B dopants and N defects have been successfully incorporated into g-C_3N_4 nanosheets by using a solid-state thermal treatment of $NaBH_4$, which could also significantly affect the catalytic performance.

Unraveling the Interfacial Interaction in Photo/Electrocatalysts. Aside from the direct utility as photo/electrocatalysts, 2D semiconductors have also been combined with other nanomaterials to fabricate efficient composite photo/electrocatalysts by assimilating and integrating their respective advantages for a superposed effect on the catalytic activity.[26,27,75] On the other hand, it is well known that the tight interfacial contact is very essential to remarkably improve the catalytic performance of composite by reducing the charge across resistance.[79-81] Therefore, by probing the fine structure of chemical bonding, soft XAS has been extensively adopted to unravel the chemical interaction in composite photo/electrocatalysts to clearly demonstrate their working mechanisms.

Recently, through a multi-interfacial engineering route, Zeng et al. constructed a strongly coupled interactive transmission network containing TiO_2, Ti_3C_2 MXene, and carbon nitride nanosheets (CNS).[82] It's worth noting that owing to the strong coupling effect, the as-obtained TiO_2/Ti_3C_2/CNS triple hybrid exhibited a stable and efficient photocatalytic activity. On the other hand, to understand the structure-activity relationship in more detail, soft XAS measurements were employed to investigate the interfacial interaction in the as-fabricated composite. As shown in Figure 8a, the C K-edge XAS spectrum of CNS showed three prominent features at about 288.5, 285.2, and 295.0 eV, which could be ascribed to the π^* excitation of N-C=N bond, the π^* excitation of C=C bond of carbon ring, and C-N σ^* orbital, respectively.[74,83] Moreover, in contrast with CNS, the position of N-C=N peak in TiO_2/Ti_2C_3/CNS composite slightly shifted to a lower energy, and meanwhile the peak intensity also obviously decreased, which originated from the breakdown of surface suspension bonds and substantial electron transfer between d ifferent phases.[84] Figure 8b depicts the N K-edge XAS spectra of all samples, in which two main π* resonance peaks at 399.2 and 402.3 eV were observed for the C=N-C and N(-C)$_3$ bonds, respectively.[85] A broad feature of σ* excitation at 404 eV assigned to the C-N bonds was also observed. More notably, due to the partial broken of C=N-C bond in the construction of TiO_2/Ti_3C_2/CNS composite, the intensity of prominent peaks also greatly reduced. A slight shift in the peak of π* resonance was found in the N K-edge XAS spectrum of TiO_2/Ti_3C_2/CNS, suggesting that owing to the perturbations of N atoms originated from the strong interaction between various components, the electron was transferred from CNS to TiO_2 via MXene. Figure 8c illustrates the Ti L-edge XAS spectra of as-obtained samples, wherein the oxidation state of Ti atoms in both TiO_2/Ti_3C_2 and TiO_2/Ti_3C_2/CNS was Ti^{4+} with $3d^0$ configuration, confirming the generation of TiO_2 through the hydrothermal oxidation of Ti_3C_2 MXene. Furthermore, the energy positions of Ti $L_{2,3}$ peaks shifted to higher values after the introduction of CNS, thus indicating a strong chemical interaction between different components in the composite, which facilitated the charge transfer. All these soft XAS results provide interesting details for understanding the structure-activity relationship in the TiO_2/Ti_3C_2/CNS composite.

Tong et al. also demonstrated a strongly coupled hybrid electro-catalyst comprising the CoO_x nanoparticles with rich oxygen vacancies and the B, N-decorated graphene (CoO_x NPs/BNG).[86] Notably, owing to the synergistic effect, the as-fabricated hybrid sample exhibited a superior OER catalytic activity with low overpotential and Tafel slope. In that study, C and N K-edge XAS characterizations were utilized to gain the insights into the interaction between CoO_x nanoparticles and B, N-decorated graphene. For C K-edge XAS measurements, the results showed that in comparison of N-incorporated graphene (NG) nanosheet, the CoO_x NPs/BNG sample showed a weaker intensity for π* transitions and a slight shift to lower energy. Additionally, a sharply increased intensity for the peak at ~287.4 eV was also observed. All these alters strongly suggested that in the hybrid, there is a strong interfacial interaction between CoO_x nanoparticles and B, N-incorporated graphene nanosheets through the formation of Co-N-C bonds.[87] Moreover, the declined intensity and lower energy position of π* transitions for CoO_x NPs/BNG further indicted the charge transfer from cobalt ions into the carbon sites of the honeycomb lattice with the bridged N. This conclusion has also been verified by N K-edge XAS spectra, where N-incorporated graphene (NG) presented several dominant N-doping sites (peaks a, b, and c) attributed to the π^* contribution from pyridinic-N, pyrrolic-N, and graphitic-N, respectively. For the CoO_x NPs/BNG hybrid, different features in N K-edge XAS spectrum were obviously found. In detail, after the introduc-

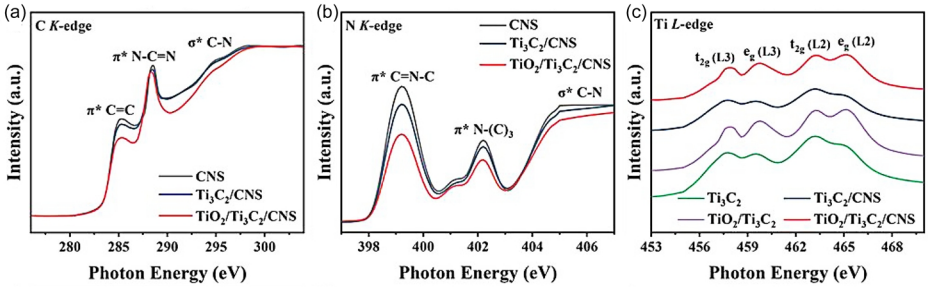

Figure 8. (a) C K-edge, (b) N K-edge, and (c) Ti L-edge XAS spectra for CNS, Ti_3C_2 /CNS, and TiO_2/Ti_3C_2/CNS samples. Reproduced with permission from Ref. [82].

DOI: 10.14102/j.cnki.0254-5861.2022-0099

tion of CoO_x nanoparticles, the intensities of peaks a and b remarkably increased. In the meantime, the energies shifted to lower values. These results further confirmed that in the hybrid, the Co-N-C bonds have been created at the pyridinic-N and pyrrolic-N sites due to the charge transfer from the Co ions into the N-decorated graphene. In summary, the C and K-edge XAS spectra clearly showed a strong interfacial interaction between CoO_x NPs and BNG via the formation of Co-N-C bonding, which favored a faster electron transfer.

Likewise, by performing C K-edge XAS characterization, an interfacial chemical bond of "C-O-Mo" in the graphdiyne/molybdenum oxide (GDY/MoO_3) composite electrocatalyst was also clearly revealed.[88] As shown in Figure 9a, the C K-edge XAS spectrum of pristine GDY shows four main peaks: A, A″, B, and C at about 285.0, 285.9, 288.3, and 293.0 eV, respectively. Therein, peaks A and C could be assigned to the π* excitation and σ* excitation of aromatic carbon-carbon bonds in a six-membered carbon ring, respectively.[89,90] The peak A″ could be related to carbon-carbon triple bonds, and peak B is associated to oxygenated functional groups such as carboxylate. Compared to the pristine GDY, a strong peak A′ for GDY/MoO_3 could be observed, manifesting the migration of electron cloud to the triple bonds attached to the carbon ring of GDY.[89,90] In addition, it also suggested that the sp-hybridized carbon atoms were involved in the C-O-Mo bonds. Subsequent electrochemical experiments and DFT calculation further showed that the formation of "sp C-O-Mo hybridization" could create new intrinsic active sites (nonoxygen vacancy sites) and simultaneously increase the number of active sites (Figure 9b), consequently achieving an outstanding HER activity via facilitating the electron transfer and improving the H_2O dissociation.

More recently, single atoms (SAs) catalysts have been developed for different catalytic reactions on account of their unique electronic properties.[8,38] Meanwhile, the anchoring of SAs on the ultrathin support, such as 2D semiconductors for the maximum atom efficiency and extraordinary catalytic properties, has also been widely reported.[38,91] For example, Hu et al. fabricated a single-atom Pt dispersed C_3N_4 (Pt SAs/C_3N_4) composite photocatalyst by an ammonia-assisted immobilization of Pt sources with C_3N_4 as supports, which exhibited an improved photocatalytic performance comparing with the pristine g-C_3N_4 nanosheets.[91] In that study, soft XAS has been adopted to probe the interfacial interaction between Pt SAs and C_3N_4 nanosheets. Similar features in the C and N K-edge XAS spectra for both pristine C_3N_4 and Pt SAs/C_3N_4 revealed that the typical graphite C_3N_4 structure was well maintained after the anchoring of Pt SAs. In addition, a noticeable positive shift in the photon energy of N K-edge XAS spectrum for Pt SAs/C_3N_4 was observed when compared to the pristine C_3N_4 counterpart. Considering the hard XAS results have clearly revealed that the isolated Pt SAs are bonded to the N atoms to form a Pt-N_3 structure, the shift in N K-edge XAS spectrum for Pt SAs/C_3N_4 could be attributed to the strong electronic interaction of nitrogen with the single-atom Pt. These results suggested that a strong electronic interaction between Pt SAs and C_3N_4 nanosheets has been successfully created by generating the Pt-N coordination bonds, which serves as a bridge to effectively shorten the carriers' diffusion length and promote the charge separation, eventually leading to an accelerated photocatalytic performance. This work shows the great potential of soft XAS in unraveling the working mechanism of single atoms/2D semiconductors photo/electrocatalysts.

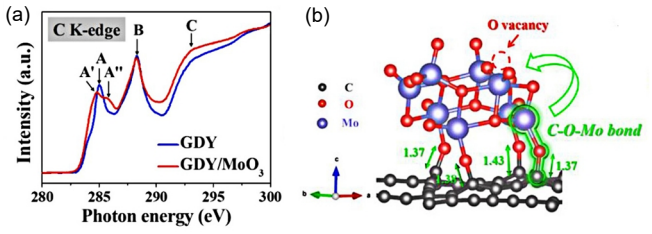

Figure 9. (a) C K-edge XAS spectra of GDY and GDY/MoO_3 samples. (b) Relationship between C-O-Mo bonds and active sites: C-O-Mo bonds at the interface between MoO_3 and GDY (green two-way arrows represent bond length, unit: angstrom). Reproduced with permission from Ref. [88].

Soft XAS has also been utilized to probe the interaction of embedded interface like core-shell structures in 2D photo/electrocatalysts.[92] For instance, Li et al fabricated a hexagonal metallic Co@N-doped graphene (hcp-Co@NC) core-shell hybrid through a controllable "phase mediation" strategy, which exhibited significantly enhanced HER and OER activities.[92] Moreover, to gain an insight into the interaction between Co core and NC shell, the electronic structure of hcp-Co@NC sample was investigated by combining the soft and hard XAS characterizations with different detection depths. In that study, the C-K edge and N K-edge XAS spectra showed characteristic peaks of C-Co and N-Co bonds in NC shell, indicating the coexistence of C-C and C-N coordination in the as-fabricated sample. In the meantime, the Fourier transform (FT) of the Co K-edge EXAFS $k^3\chi(k)$ oscillation curves also showed the existence of C-Co peak and a weak peak at the same position as that for the C-C/N bond in the reference Co(II) phthalocyanine (CoPc) sample. All the results clearly revealed the formation of C-C/N bonds at the interface between Co core and NC shell in the hcp-Co@NC hybrid, which provided solid evidence for understanding its working mechanism.

Soft XAS for 2D Nanomaterials-Based Photoelectrocatalytic Water Splitting. By combining the advantages of photocatalytic and electrocatalytic water splitting, photoelectrocatalytic/photoelectrochemical (PEC) water splitting holds more promise in achieving highly efficient hydrogen production.[7,15,93] In PEC water splitting system, photoelectrodes involving photoanode and photocathode are the key components, which determine the conversion efficiency of solar-to-hydrogen (STH) of the whole system.[15,93] Since the pioneer work reported in 1972,[94] major efforts have been devoted to fabricating highly efficient photoelectrodes to meet the demand of practical application. Until now, numerous semiconductors such as metal oxides, sulfides, and nitrides have been exploited to be photoelectrodes for solar-driven water splitting.[2,36,37,93] Amongst, 2D nanomaterials have displayed greater potential owing to their unique structures, which as the photo-electrodes for PEC water splitting have also been widely reported.[12,14,15] Also, soft XAS has been extensively used to explore the working mechanism of these 2D photoelectrodes by probing their electronic structure and bonding infor-

Chin. J. Struct. Chem. **2022**, 41, 2210016-2210028
DOI: 10.14102/j.cnki.0254-5861.2022-0099

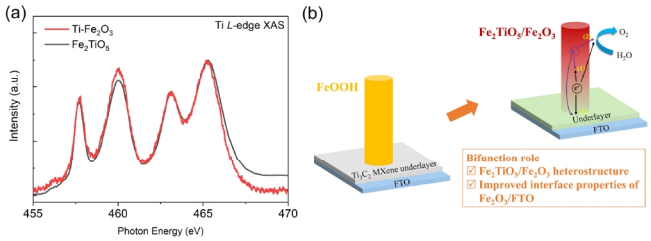

Figure 10. (a) Ti L-edge XAS spectra of Ti_3C_2 MXene underlayer modified hematite (Ti-Fe_2O_3) photoanode and Fe_2TiO_5 reference. (b) Schematic of the working mechanism of Ti-Fe_2O_3 photoanode. Reproduced with permission from Ref. [96].

mation.

Yan et al. recently demonstrated a 0D/2D van der Waals heterojunction by integrating N and S co-doped graphene quantum dots (GQDs) with pristine graphene nanosheets through the ultrasonication of graphite powder with GQDs as intercalation surfactant.[95] When using the as-fabricated heterojunction as the photoelectrode for water splitting, a high PEC performance was obtained because of the combined merits. In that study, soft XAS at C K-edge was performed to confirm the electronic coupling in the 0D/2D heterojunction to provide more insights into its working mechanism. The XAS results clearly demonstrated that compared to pristine graphene, there is an apparent shift for the C=C peak toward lower photon energy in both GQD/graphene and NS-GQD/graphene samples. Notably, the shift caused by NS-GQDs was more prominent than that by undoped GQDs. These findings manifested the charge transfer from GQDs to graphene, which was further facilitated by N and S co-doping. Thus, the charge transfer could lower the work function and increase the carrier density, eventually resulting in an improved PEC activity.

By using a drop-casting method followed by hydrothermal and sintering processes, recently we have also fabricated a Ti_3C_2 MXene underlayer modified hematite (Ti-Fe_2O_3) photoanode for water splitting, which showed an increased photocurrent density compared to that of the pristine Fe_2O_3 sample.[96] Ti L-edge XAS measurements for Ti-Fe_2O_3 and the pristine Fe_2O_3 photoanodes have been carried out to clarify the chemical states of Ti species in the Ti-Fe_2O_3 photoanode. As shown in Figure 10a, the Ti-Fe_2O_3 photoanode exhibited a Ti L-edge XAS spectrum similar to that of Fe_2TiO_5 reference, suggesting that the Ti species in Ti-Fe_2O_3 photoanode mainly existed as Fe_2TiO_5. In fact, previous reports have demonstrated that Ti ions could diffuse from Ti-based underlayer into hematite through a sintering process at high temperature.[97,98] Therefore, the generation of Fe_2TiO_5 in Ti-Fe_2O_3 photoanode could be assigned to the Ti^{4+} diffusion from the Ti_3C_2 MXene underlayer to hematite nanostructures in the subsequent sintering at high temperature. Consequently, due to the bifunctional role of Ti_3C_2 MXene underlayer in improving FTO/hematite interfacial properties and providing Ti source for building the Fe_2TiO_5/Fe_2O_3 heterostructure, the charge transfer kinetics could be greatly accelerated, achieving an improved photocurrent density as shown in Figure 10b.

Additionally, soft XAS has also been employed to study the chemical compositions in C_3N_4-based photoelectrodes to gain a better understanding of their catalytic properties. For example, Zhang et al. reported a facile liquid-mediated method for the fabrication of nickel embedded and phenyl-modified C_3N_4 photoanode.[99] C and N K-edge as well as Ni L-edge XAS measurements have been conducted to investigate the electronic structures of as-synthesized samples. The XAS data clearly revealed that for the optimal photoanode, the Ni ions had an oxidation state of 2.8, which could not only sever as very active electrocatalysts but also strongly enhance the light absorption in the visible region, consequently resulting in a high PEC performance. This work offered a guide for the fabrication of high-efficient g-C_3N_4-based photoelectrodes for water splitting.

n CONCLUSIONS AND PERSPECTIVES

Nowadays, 2D nanomaterials as the newly emerging materials have attracted increasing interests, and their applications in photo/electrocatalytic water splitting have also been one of the research focuses. Compared with traditional bulk and other nano-sized catalysts, 2D nanomaterials possess plenty of impressive characteristics, including large specific surface area, abundant active sites, excellent conductivity, and tunable bandgap, which render them promising candidates for photo/electrocatalytic water splitting. Furthermore, considerable efforts have also been taken to significantly boost their photo/electrocatalytic activities and stabilities, such as element doping, surface engineering, and composite/heterostructure building. Nevertheless, currently, the development of high-efficient 2D photo/electrocatalysts for water splitting is still a great challenge. One critical cause is the lack of strong experimental evidences and sufficient theoretical insights to understand their working mechanisms deeply and comprehensively. In such case, synchrotron-based XAS as a powerful tool opens a novel, feasible and efficient way to explore the electronic structure and bonding environments of 2D photo/electrocatalysts, enormously facilitating the development of this area. Therefore, in this review, via overviewing the recent achievements of synchrotron-based soft XAS applied in 2D nanomaterials for photo/electrocatalytic water splitting and highlighting some of the salient results acquired from these experiments, we provide an insight into how soft XAS can instruct the fabrication of efficient 2D photo/electrocatalysts by identifying the surface active sites, elucidating the heteroatoms' location, and unraveling the interfacial interaction.

In the meantime, we also note that despite soft XAS has shown great potential in demonstrating the reactive mechanism of 2D photo/electrocatalysts, its application is still at an early stage and there are significant challenges that need to be overcome in future studies. First, soft XAS still suffers from several inherent limitations, such as the carbon contamination existing in the optical devices of beamline or the sample surface which could lower the quality of as-obtained spectra and complicate the data analysis especially at the C K-edge. Second, in comparison with ex-situ soft XAS characterizations, in-situ/operando soft XAS techniques can provide more information on the working mechanism of 2D photo/electrocatalysts by monitoring the electronic structure changes under real reaction conditions. However, owing to the ultra-high vacuum environment and the low detec-

DOI: 10.14102/j.cnki.0254-5861.2022-0099

tion depth of soft XAS, the utilization of in-situ/operando soft XAS is still a great challenge. Therefore, the design of more effective in-situ cell/reactor that could yield high-quality and authentic experimental data is highly required. Third, until now, none of the characterization tools can comprehensively and deeply unravel the structure-property relationship of 2D photo/electrocatalysts. Consequently, the combination of soft XAS with other advanced characterization techniques, such as hard XAS, ambient pressure X-ray photoelectron spectroscopy (APXPS), aberration-corrected scanning transmission electron microscopy (STEM), etc. should be given more attention. It is believed that with the development of new generation (e.g., 4th) synchrotron sources with higher flux and better time-resolution, soft XAS as a powerful and element-specific tool will play an increasingly greater role in guiding the fabrication of high-performance photo/electrocatalysts for water splitting.

n ACKNOWLEDGEMENTS

This work was financially supported by National Key R&D Program of China (2020YFA0406103), China Postdoctoral Science Foundation (2020T130754), and National Natural Science Foundation of China (51902139, U1932211).

n AUTHOR INFORMATION

Corresponding authors. Emails: jjDeng@ujs.edu.cn (J. Deng) and jZhong@suda.edu.cn (J. Zhong)

n COMPETING INTERESTS

The authors declare no competing interests.

n ADDITIONAL INFORMATION

Full paper can be accessed via
http://manu30.magtech.com.cn/jghx/EN/10.14102/j.cnki.0254-5861.2022-0099
For submission: https://www.editorialmanager.com/cjschem

n REFERENCES

(1) Turner, J. A. Sustainable hydrogen production. *Science* **2004**, 305, 972-974.
(2) Osterloh, F. E. Inorganic nanostructures for photoelectrochemical and photocatalytic water splitting. *Chem. Soc. Rev.* **2013**, 42, 2294-2320.
(3) Wang, Z.; Li, C.; Domen, K. Recent developments in heterogeneous photocatalysts for solar-driven overall water splitting. *Chem. Soc. Rev.* **2019**, 48, 2109-2125.
(4) Li, Z.; Hu, M.; Wang, P.; Liu, J.; Yao, J.; Li, C. Heterojunction catalyst in electrocatalytic water splitting. *Coord. Chem. Rev.* **2021**, 439, 213953.
(5) Li, Y.; Sun, Y.; Qin, Y.; Zhang, W.; Wang, L.; Luo, M.; Yang, H.; Guo, S. Recent advances on water-splitting electrocatalysis mediated by noble-metal-based nanostructured materials. *Adv. Energy Mater.* **2020**, 10, 1903120.
(6) Yan, Y.; Wang, P.; Lin, J.; Cao, J.; Qi, J. Modification strategies on transition metal-based electrocatalysts for efficient water splitting. *J. Energy Chem.* **2021**, 58, 446-462.
(7) Li, C.; Luo, Z.; Wang, T.; Gong, J. Surface, bulk, and interface: rational design of hematite architecture toward efficient photo-electrochemical water splitting. *Adv. Mater.* **2018**, 30, 1707502.
(8) Sultan, S.; Tiwari, J. N.; Singh, A. N.; Zhumagali, S.; Ha, M.; Myung, C. W.; Thangavel, P.; Kim, K. S. Single atoms and clusters based nanomaterials for hydrogen evolution, oxygen evolution reactions, and full water splitting. *Adv. Energy Mater.* **2019**, 9, 1900624.
(9) Zhang, Y.; Wang, D.; Wang, S. High-entropy alloys for electrocatalysis: design, characterization, and applications. *Small* **2021**, 18, 2104339.
(10) Yao, L.; Rahmanudin, A.; Guijarro, N.; Sivula, K. Organic semiconductor based devices for solar water splitting. *Adv. Energy Mater.* **2018**, 8, 1802585.
(11) Di, J.; Yan, C.; Handoko, A. D.; Seh, Z. W.; Li, H.; Liu, Z. Ultrathin two-dimensional materials for photo- and electrocatalytic hydrogen evolution. *Mater. Today* **2018**, 21, 749-770.
(12) Zhou, M.; Lou, X. W. D.; Xie, Y. Two-dimensional nanosheets for photoelectrochemical water splitting: possibilities and opportunities. *Nano Today* **2013**, 8, 598-618.
(13) Deng, D.; Novoselov, K.; Fu, Q.; Zheng, N.; Tian, Z.; Bao, X. Catalysis with two-dimensional materials and their heterostructures. *Nat. Nanotechnol.* **2016**, 11, 218-230.
(14) Faraji, M.; Yousefi, M.; Yousefzadeh, S.; Zirak, M.; Naseri, N.; Jeon, T. H.; Choi, W.; Moshfegh, A. Z. Two-dimensional materials in semiconductor photoelectrocatalytic systems for water splitting. *Energy Environ. Sci.* **2019**, 12, 59-95.
(15) Ke, J.; He, F.; Wu, H.; Lyu, S.; Liu, J.; Yang, B.; Li, Z.; Zhang, Q.; Chen, J.; Lei, L. Nanocarbon-enhanced 2D photoelectrodes: a new paradigm in photoelectrochemical water splitting. *Nano-Micro Lett.* **2021**, 13, 1-29.
(16) Zhang, H. Ultrathin two-dimensional nanomaterials. *ACS Nano* **2015**, 9, 9451-9469.
(17) Wang, H.; Liu, X.; Niu, P.; Wang, S.; Shi, J.; Li, L. Porous two-dimensional materials for photocatalytic and electrocatalytic applications. *Matter* **2020**, 2, 1377-1413.
(18) Zhang, Y.; Li, L.; Guo, S. X.; Zhang, X.; Li, F.; Bond, A. M.; Zhang, J. Two-dimensional electrocatalysts for efficient reduction of carbon dioxide. *ChemSusChem* **2020**, 13, 59-77.
(19) Yin, T.; Long, L.; Tang, X.; Qiu, M.; Liang, W.; Cao, R.; Zhang, Q.; Wang, D.; Zhang, H. Advancing applications of black phosphorus and BP-analog materials in photo/electrocatalysis through structure engineering and surface modulation. *Adv. Sci.* **2020**, 7, 2001431.
(20) Qian, W.; Xu, S.; Zhang, X.; Li, C.; Yang, W.; Bowen, C. R.; Yang, Y. Differences and similarities of photocatalysis and electrocatalysis in two-dimensional nanomaterials: strategies, traps, applications and challenges. *Nano-Micro Lett.* **2021**, 13, 1-38.
(21) Ling, Z.; Ren, C. E.; Zhao, M.-Q.; Yang, J.; Giammarco, J. M.; Qiu, J.; Barsoum, M. W.; Gogotsi, Y. Flexible and conductive MXene films and nanocomposites with high capacitance. *Proc. Natl. Acad. Sci.* **2014**, 111, 16676-16681.
(22) Zhang, X.; Chen, A.; Chen, L.; Zhou, Z. 2D materials bridging experiments and computations for electro/photocatalysis. *Adv. Energy Mater.* **2022**, 12, 2003841.
(23) Sun, Y.; Gao, S.; Lei, F.; Xie, Y. Atomically-thin two-dimensional sheets for understanding active sites in catalysis. *Chem. Soc. Rev.* **2015**, 44, 623-636.
(24) Yi, J.; El-Alami, W.; Song, Y.; Li, H.; Ajayan, P. M.; Xu, H. Emerging surface strategies on graphitic carbon nitride for solar driven water splitting. *Chem. Eng. J.* **2020**, 382, 122812.
(25) Boumeriame, H.; Da Silva, E. S.; Cherevan, A. S.; Chafik, T.; Faria, J.

L.; Eder, D. Layered double hydroxide (LDH)-based materials: a mini-review on strategies to improve the performance for photocatalytic water splitting. *J. Energy Chem.* **2022**, 64, 406-431.
(26) Zhao, D.; Wang, Y.; Dong, C.-L.; Huang, Y.-C.; Chen, J.; Xue, F.; Shen, S.; Guo, L. Boron-doped nitrogen-deficient carbon nitride-based Z-scheme heterostructures for photocatalytic overall water splitting. *Nat. Energy* **2021**, 6, 388-397.
(27) Yuan, Z.; Li, J.; Yang, M.; Fang, Z.; Jian, J.; Yu, D.; Chen, X.; Dai, L. Ultrathin black phosphorus-on-nitrogen doped graphene for efficient overall water splitting: dual modulation roles of directional interfacial charge transfer. *J. Am. Chem. Soc.* **2019**, 141, 4972-4979.
(28) Li, S.; Zhang, Y.; Huang, H. Black phosphorus-based heterostructures for photocatalysis and photoelectrochemical water splitting. *J. Energy Chem.* **2022**, 67, 745-779.
(29) Luo, C.; Wang, C.; Wu, X.; Zhang, J.; Chu, J. In situ transmission electron microscopy characterization and manipulation of two-dimensional layered materials beyond graphene. *Small* **2017**, 13, 1604259.
(30) Fang, L.; Seifert, S.; Winans, R. E.; Li, T. Understanding synthesis and structural variation of nanomaterials through in situ/operando XAS and SAXS. *Small* **2022**, 18, 2106017.
(31) Smith, J. W.; Saykally, R. J. Soft X-ray absorption spectroscopy of liquids and solutions. *Chem. Rev.* **2017**, 117, 13909-13934.
(32) Timoshenko, J.; Roldan Cuenya, B. In situ/operando electrocatalyst characterization by X-ray absorption spectroscopy. *Chem. Rev.* **2020**, 121, 882-961.
(33) Zhong, J.; Zhang, H.; Sun, X.; Lee, S. T. Synchrotron soft X-ray absorption spectroscopy study of carbon and silicon nanostructures for energy applications. *Adv. Mater.* **2014**, 26, 7786-7806.
(34) Deng, J.; Zhang, Q.; Lv, X.; Zhang, D.; Xu, H.; Ma, D.; Zhong, J. Understanding photoelectrochemical water oxidation with X-ray absorption spectroscopy. *ACS Energy Lett.* **2020**, 5, 975-993.
(35) Liu, X.; Weng, T.-C. Synchrotron-based X-ray absorption spectroscopy for energy materials. *MRS Bull.* **2016**, 41, 466-472.
(36) Cho, S.; Jang, J.-W.; Lee, K.-H.; Lee, J. S. Research update: strategies for efficient photoelectrochemical water splitting using metal oxide photoanodes. *APL Mater.* **2014**, 2, 010703.
(37) Hisatomi, T.; Kubota, J.; Domen, K. Recent advances in semiconductors for photocatalytic and photoelectrochemical water splitting. *Chem. Soc. Rev.* **2014**, 43, 7520-7535.
(38) Li, P.; Zhao, G.; Cui, P.; Cheng, N.; Lao, M.; Xu, X.; Dou, S. X.; Sun, W. Nickel single atom-decorated carbon nanosheets as multifunctional electrocatalyst supports toward efficient alkaline hydrogen evolution. *Nano Energy* **2021**, 83, 105850.
(39) Weng, Q.; Kvashnin, D. G.; Wang, X.; Cretu, O.; Yang, Y.; Zhou, M.; Zhang, C.; Tang, D. M.; Sorokin, P. B.; Bando, Y. Tuning of the optical, electronic, and magnetic properties of boron nitride nanosheets with oxygen doping and functionalization. *Adv. Mater.* **2017**, 29, 1700695.
(40) Wang, B.; Chu, S.; Zheng, L.; Li, X.; Zhang, J.; Zhang, F. Application of X-ray absorption spectroscopy in electrocatalytic water splitting and CO_2 reduction. *Small Sci.* **2021**, 1, 2100023.
(41) Timoshenko, J.; Cuenya, B. R. In situ/operando electrocatalyst characterization by X-ray absorption spectroscopy. *Chem. Rev.* **2021**, 121, 882-961.
(42) Chen, M.; Chou, S. L.; Dou, S. X. Understanding challenges of cathode materials for sodium-ion batteries using synchrotron-based X-ray absorption spectroscopy. *Batteries Supercaps* **2019**, 2, 842-851.
(43) Nagasaka, M.; Kosugi, N. Soft X-ray absorption spectroscopy for observing element-specific intermolecular interaction in solution chemistry. *Chem. Lett.* **2021**, 50, 956-964.
(44) Che, W.; Cheng, W.; Yao, T.; Tang, F.; Liu, W.; Su, H.; Huang, Y.; Liu, Q.; Liu, J.; Hu, F. Fast photoelectron transfer in (C_{ring})-C_3N_4 plane heterostructural nanosheets for overall water splitting. *J. Am. Chem. Soc.* **2017**, 139, 3021-3026.
(45) Zhao, J.; Zhang, J. J.; Li, Z. Y.; Bu, X. H. Recent progress on NiFe-based electrocatalysts for the oxygen evolution reaction. *Small* **2020**, 16, 2003916.
(46) Gong, L.; Yang, H.; Douka, A. I.; Yan, Y.; Xia, B. Y. Recent progress on NiFe-based electrocatalysts for alkaline oxygen evolution. *Adv. Sustain. Syst.* **2021**, 5, 2000136.
(47) Stevens, M. B.; Trang, C. D.; Enman, L. J.; Deng, J.; Boettcher, S. W. Reactive Fe-sites in Ni/Fe (oxy)hydroxide are responsible for exceptional oxygen electrocatalysis activity. *J. Am. Chem. Soc.* **2017**, 139, 11361-11364.
(48) Ahn, H. S.; Bard, A. J. Surface Interrogation scanning electrochemical microscopy of $Ni_{1-x}Fe_xOOH$ ($0<x<0.27$) oxygen evolving catalyst: kinetics of the "fast" iron sites. *J. Am. Chem. Soc.* **2016**, 138, 313-318.
(49) Louie, M. W.; Bell, A. T. An Investigation of thin-film Ni-Fe oxide catalysts for the electrochemical evolution of oxygen. *J. Am. Chem. Soc.* **2013**, 135, 12329-12337.
(50) Friebel, D.; Louie, M. W.; Bajdich, M.; Sanwald, K. E.; Cai, Y.; Wise, A. M.; Cheng, M.-J.; Sokaras, D.; Weng, T.-C.; Alonso-Mori, R. Identification of highly active Fe sites in (Ni, Fe)OOH for electrocatalytic water splitting. *J. Am. Chem. Soc.* **2015**, 137, 1305-1313.
(51) Chen, J. Y.; Dang, L.; Liang, H.; Bi, W.; Gerken, J. B.; Jin, S.; Alp, E. E.; Stahl, S. S. Operando analysis of NiFe and Fe oxyhydroxide electrocatalysts for water oxidation: detection of Fe^{4+} by Mossbauer spectroscopy. *J. Am. Chem. Soc.* **2015**, 137, 15090-15093.
(52) Chen, S.; Kang, Z.; Zhang, X.; Xie, J.; Wang, H.; Shao, W.; Zheng, X.; Yan, W.; Pan, B.; Xie, Y. Highly active Fe sites in ultrathin pyrrhotite Fe_7S_8 nanosheets realizing efficient electrocatalytic oxygen evolution. *ACS Cent. Sci.* **2017**, 3, 1221-1227.
(53) Long, X.; Wang, Z.; Xiao, S.; An, Y.; Yang, S. Transition metal based layered double hydroxides tailored for energy conversion and storage. *Mater. Today* **2016**, 19, 213-226.
(54) Dionigi, F.; Zhu, J.; Zeng, Z.; Merzdorf, T.; Sarodnik, H.; Gliech, M.; Pan, L.; Li, W.-X.; Greeley, J.; Strasser, P. Intrinsic electrocatalytic activity for oxygen evolution of crystalline 3d-transition metal layered double hydroxides. *Angew. Chem. Int. Ed.* **2021**, 60, 14446-14457.
(55) Zhao, Y.; Zhang, X.; Jia, X.; Waterhouse, G. I.; Shi, R.; Zhang, X.; Zhan, F.; Tao, Y.; Wu, L. Z.; Tung, C. H. Sub-3 nm ultrafine monolayer layered double hydroxide nanosheets for electrochemical water oxidation. *Adv. Energy Mater.* **2018**, 8, 1703585.
(56) Kang, J.; Qiu, X.; Hu, Q.; Zhong, J.; Gao, X.; Huang, R.; Wan, C.; Liu, L.-M.; Duan, X.; Guo, L. Valence oscillation and dynamic active sites in monolayer NiCo hydroxides for water oxidation. *Nat. Catal.* **2021**, 4, 1050-1058.
(57) Li, R.; Yang, S.; Zhang, Y.; Yu, G.; Wang, C.; Chen, C.; Wu, G.; Sun, R.; Wang, G.; Zheng, X. Short-range order in amorphous nickel oxide nanosheets enables selective and efficient electrochemical hydrogen peroxide production. *Cell Rep. Phys. Sci.* **2022**, 3, 100788.
(58) Kuai, C.; Zhang, Y.; Han, L.; Xin, H. L.; Sun, C.-J.; Nordlund, D.; Qiao, S.; Du, X.-W.; Lin, F. Creating compressive stress at the NiOOH/NiO interface for water oxidation. *J. Mater. Chem. A* **2020**, 8, 10747-

DOI: 10.14102/j.cnki.0254-5861.2022-0099

10754.
(59) Rabchinskii, M. K.; Saveliev, S. D.; Stolyarova, D. Y.; Brzhezinskaya, M.; Kirilenko, D. A.; Baidakova, M. V.; Ryzhkov, S. A.; Shnitov, V. V.; Sysoev, V. V.; Brunkov, P. N. Modulating nitrogen species via N-doping and post annealing of graphene derivatives: XPS and XAS examination. *Carbon* **2021**, 182, 593-604.
(60) Zhao, B.; Feng, K.; Wang, Y.; Lv, X.; Zheng, H.; Ma, Y.; Yan, W.; Sun, X.; Zhong, J. $Pt_xNi_{10-x}O$ nanoparticles supported on N-doped graphene oxide with a synergetic effect for highly efficient hydrolysis of ammonia borane. *Catal. Sci. Technol.* **2017**, 7, 5135-5142.
(61) Yang, H.; Miao, J.; Hung, S.; Chen, J.; Tao, H.; Wang, X.; Zhang, L.; Chen, R.; Gao, J.; Chen, H. Identification of catalytic sites for oxygen reduction and oxygen evolution in N-doped graphene bifunctional electrocatalysts. *Sci. Adv.* **2016**, 2, e1501122.
(62) Liu, G.; Niu, P.; Sun, C.; Smith, S. C.; Chen, Z.; Lu, G. Q.; Cheng, H.-M. Unique electronic structure induced high photoreactivity of sulfur-doped graphitic C_3N_4. *J. Am. Chem. Soc.* **2010**, 132, 11642-11648.
(63) Zou, J.; Liao, G.; Jiang, J.; Xiong, Z.; Bai, S.; Wang, H.; Wu, P.; Zhang, P.; Li, X. In-situ construction of sulfur-doped g-C_3N_4/defective g-C_3N_4 isotype step-scheme heterojunction for boosting photocatalytic H_2 evolution. *Chin. J. Struct. Chem.* **2022**, 41, 2201025-2201033.
(64) Patnaik, S.; Sahoo, D. P.; Parida, K. Recent advances in anion doped g-C_3N_4 photocatalysts: a review. *Carbon* **2021**, *172*, 682-711.
(65) Gu, J.; Magagula, S.; Zhao, J.; Chen, Z. Boosting ORR/OER activity of graphdiyne by simple heteroatom doping. *Small Methods* **2019**, 3, 1800550.
(66) Li, G.; Li, Y.; Liu, H.; Guo, Y.; Li, Y.; Zhu, D. Architecture of graphdiyne nanoscale films. *Chem. Commun.* **2010**, 46, 3256-3258.
(67) Zhao, Y.; Wan, J.; Yao, H.; Zhang, L.; Lin, K.; Wang, L.; Yang, N.; Liu, D.; Song, L.; Zhu, J. Few-layer graphdiyne doped with sp-hybridized nitrogen atoms at acetylenic sites for oxygen reduction electrocatalysis. *Nat. Chem.* **2018**, 10, 924-931.
(68) Zhao, Y.; Yang, N.; Yao, H.; Liu, D.; Song, L.; Zhu, J.; Li, S.; Gu, L.; Lin, K.; Wang, D. Stereodefined codoping of sp-N and S atoms in few-layer graphdiyne for oxygen evolution reaction. *J. Am. Chem. Soc.* **2019**, 141, 7240-7244.
(69) Chen, X.; Ong, W.-J.; Kong, Z.; Zhao, X.; Li, N. Probing the active sites of site-specific nitrogen doping in metal-free graphdiyne for electrochemical oxygen reduction reactions. *Sci. Bull.* **2020**, 65, 45-54.
(70) Subbaraman, R.; Tripkovic, D.; Chang, K.-C.; Strmcnik, D.; Paulikas, A. P.; Hirunsit, P.; Chan, M.; Greeley, J.; Stamenkovic, V.; Markovic, N. M. Trends in activity for the water electrolyser reactions on 3*d* M (Ni, Co, Fe, Mn) hydr(oxy)oxide catalysts. *Nat. Mater.* **2012**, 11, 550-557.
(71) Li, S.; Hao, X.; Abudula, A.; Guan, G. Nanostructured Co-based bifunctional electrocatalysts for energy conversion and storage: current status and perspectives. *J. Mater. Chem. A* **2019**, 7, 18674-18707.
(72) Huang, Y.; Zhao, X.; Tang, F.; Zheng, X.; Cheng, W.; Che, W.; Hu, F.; Jiang, Y.; Liu, Q.; Wei, S. Strongly electrophilic heteroatoms confined in atomic CoOOH nanosheets realizing efficient electrocatalytic water oxidation. *J. Mater. Chem. A* **2018**, 6, 3202-3210.
(73) Tufts, B. J.; Abrahams, I. L.; Caley, C. E.; Lunt, S. R.; Miskelly, G. M.; Sailor, M. J.; Santangelo, P. G.; Lewis, N. S.; Roe, A. L.; Hodgson, K. O. XPS and EXAFS studies of the reactions of cobalt (III) ammine complexes with gallium arsenide surfaces. *J. Am. Chem. Soc.* **1990**, 112, 5123-5136.
(74) Zhao, D.; Dong, C. L.; Wang, B.; Chen, C.; Huang, Y. C.; Diao, Z.; Li, S.; Guo, L.; Shen, S. Synergy of dopants and defects in graphitic carbon nitride with exceptionally modulated band structures for efficient photocatalytic oxygen evolution. *Adv. Mater.* **2019**, 31, 1903545.
(75) Ran, J.; Guo, W.; Wang, H.; Zhu, B.; Yu, J.; Qiao, S.-Z. Metal-free 2D/2D phosphorene/g-C_3N_4 van der Waals heterojunction for highly enhanced visible-light photocatalytic H_2 production. *Adv. Mater.* **2018**, 30, 1800128.
(76) Chen, J.; Dong, C.-L.; Du, Y.; Zhao, D.; Shen, S. Nanogap engineered plasmon-enhancement in photocatalytic solar hydrogen conversion. *Adv. Mater. Interfaces* **2015**, 2, 1500280.
(77) Zhao, D.; Chen, J.; Dong, C.-L.; Zhou, W.; Huang, Y.-C.; Mao, S. S.; Guo, L.; Shen, S. Interlayer interaction in ultrathin nanosheets of graphitic carbon nitride for efficient photocatalytic hydrogen evolution. *J. Catal.* **2017**, 352, 491-497.
(78) Chen, J.; Dong, C.-L.; Zhao, D.; Huang, Y.-C.; Wang, X.; Samad, L.; Dang, L.; Shearer, M.; Shen, S.; Guo, L. Molecular design of polymer heterojunctions for efficient solar-hydrogen conversion. *Adv. Mater.* **2017**, 29, 1606198.
(79) Tang, H.; Ju, T.; Dai, Y.; Wang, M.; Wang, M.; Ma, Y.; Zheng, G. Synthesis and photocatalytic performance of BiOCl/graphene composite with tight interfacial contact and highly exposed (001) facets. *Appl. Organomet. Chem.* **2022**, 36, e6526.
(80) Lu, M.; Li, Q.; Zhang, C.; Fan, X.; Li, L.; Dong, Y.; Chen, G.; Shi, H. Remarkable photocatalytic activity enhancement of CO_2 conversion over 2D/2D g-C_3N_4/$BiVO_4$ Z-scheme heterojunction promoted by efficient interfacial charge transfer. *Carbon* **2020**, 160, 342-352.
(81) Gao, H.; Yang, H.; Xu, J.; Zhang, S.; Li, J. Strongly coupled g-C_3N_4 nanosheets-Co_3O_4 quantum dots as 2D/0D heterostructure composite for peroxymonosulfate activation. *Small* **2018**, 14, 1801353.
(82) Zeng, H.; Li, Z.; Li, G.; Cui, X.; Jin, M.; Xie, T.; Liu, L.; Jiang, M.; Zhong, X.; Zhang, Y.; Zhang, H.; Ba, K.; Yan, Z.; Wang, Y.; Song, S.; Huang, K.; Feng, S. Interfacial engineering of TiO_2/Ti_3C_2 MXene/carbon nitride hybrids boosting charge transfer for efficient photocatalytic hydrogen evolution. *Adv. Energy Mater.* **2022**, 12, 2102765.
(83) Xu, H.; She, X.; Fei, T.; Song, Y.; Liu, D.; Li, H.; Yang, X.; Yang, J.; Li, H.; Song, L. Metal-oxide-mediated subtractive manufacturing of two-dimensional carbon nitride for high-efficiency and high-yield photocatalytic H_2 evolution. *ACS Nano* **2019**, 13, 11294-11302.
(84) Zhu, Y.; Lv, C.; Yin, Z.; Ren, J.; Yang, X.; Dong, C.-L.; Liu, H.; Cai, R.; Huang, Y.-C.; Theis, W.; Shen, S.; Yang, D. A [001]-oriented Hittorf's phosphorus nanorods/polymeric carbon nitride heterostructure for boosting wide-spectrum-responsive photocatalytic hydrogen evolution from pure water. *Angew. Chem. Int. Ed.* **2020**, 59, 868-873.
(85) Han, C.; Du, L.; Konarova, M.; Qi, D.-C.; Phillips, D. L.; Xu, J. Beyond hydrogen evolution: solar-driven, water-donating transfer hydrogenation over platinum/carbon nitride. *ACS Catal.* **2020**, 10, 9227-9235.
(86) Tong, Y.; Chen, P.; Zhou, T.; Xu, K.; Chu, W.; Wu, C.; Xie, Y. A bifunctional hybrid electrocatalyst for oxygen reduction and evolution: cobalt oxide nanoparticles strongly coupled to B,N-decorated graphene. *Angew. Chem. Int. Ed.* **2017**, 56, 7121-7125.
(87) Liang, Y.; Li, Y.; Wang, H.; Zhou, J.; Wang, J.; Regier, T.; Dai, H. Co_3O_4 nanocrystals on graphene as a synergistic catalyst for oxygen reduction reaction. *Nat. Mater.* **2011**, 10, 780-786.
(88) Yao, Y.; Zhu, Y.; Pan, C.; Wang, C.; Hu, S.; Xiao, W.; Chi, X.; Fang, Y.; Yang, J.; Deng, H. Interfacial sp C-O-Mo hybridization originated high-current density hydrogen evolution. *J. Am. Chem. Soc.* **2021**, 143, 8720- 8730.
(89) Zhong, J.; Wang, J.; Zhou, J.-G.; Mao, B.-H.; Liu, C.-H.; Liu, H.-B.; Li,

DOI: 10.14102/j.cnki.0254-5861.2022-0099

Y.-L.; Sham, T.-K.; Sun, X.-H.; Wang, S.-D. Electronic structure of graphdiyne probed by X-ray absorption spectroscopy and scanning transmission X-ray microscopy. *J. Phys. Chem. C* **2013**, 117, 5931-5936.
(90) Ketabi, N.; Tolhurst, T. M.; Leedahl, B.; Liu, H.; Li, Y.; Moewes, A. How functional groups change the electronic structure of graphdiyne: theory and experiment. *Carbon* **2017**, 123, 1-6.
(91) Hu, Y.; Qu, Y.; Zhou, Y.; Wang, Z.; Wang, H.; Yang, B.; Yu, Z.; Wu, Y. Single Pt atom-anchored C_3N_4: a bridging Pt-N bond boosted electron transfer for highly efficient photocatalytic H_2 generation. *Chem. Eng. J.* **2021**, 412, 128749.
(92) Li, N.; Tan, H.; Ding, X.; Duan, H.; Hu, W.; Li, G.; Ji, Q.; Lu, Y.; Wang, Y.; Hu, F.; Wang, C.; Cheng, W.; Sun, Z.; Yan, W. Phase-mediated robust interfacial electron-coupling over core-shell Co@carbon towards superior overall water splitting. *Appl. Catal., B* **2020**, 266, 118621.
(93) Wang, Y.; Huang, J.; Wang, L.; She, H.; Wang, Q. Research progress of ferrite materials for photoelectrochemical water splitting. *Chin. J. Struct. Chem.* **2022**, 41, 2201054-2201068.
(94) Fujishima, A.; Honda, K. Electrochemical photolysis of water at a semiconductor electrode. *Nature* **1972**, 238, 37-38.
(95) Yan, Y.; Zhai, D.; Liu, Y.; Gong, J.; Chen, J.; Zan, P.; Zeng, Z.; Li, S.; Huang, W.; Chen, P. Van Der Waals heterojunction between a bottom-up grown doped graphene quantum dot and graphene for photoelectrochemical water splitting. *ACS Nano* **2020**, 14, 1185-1195.
(96) Ji, H.; Shao, S.; Yuan, G.; Lu, C.; Feng, K.; Xia, Y.; Lv, X.; Zhong, J.; Xu, H.; Deng, J. Unraveling the role of Ti_3C_2 MXene underlayer for enhanced photoelectrochemical water oxidation of hematite photoanodes. *J. Energy Chem.* **2021**, 52, 147-154.
(97) Annamalai, A.; Shinde, P. S.; Subramanian, A.; Kim, J. Y.; Kim, J. H.; Choi, S. H.; Lee, J. S.; Jang, J. S. Bifunctional TiO_2 underlayer for α-Fe_2O_3 nanorod based photoelectrochemical cells: enhanced interface and Ti^{4+} doping. *J. Mater. Chem. A* **2015**, 3, 5007-5013.
(98) Shinde, P. S.; Mahadik, M. A.; Lee, S. Y.; Ryu, J.; Choi, S. H.; Jang, J. S. Surfactant and TiO_2 underlayer derived porous hematite nanoball array photoanode for enhanced photoelectrochemical water oxidation. *Chem. Eng. J.* **2017**, 320, 81-92.
(99) Zhang, W.; Albero, J.; Xi, L.; Lange, K. M.; Garcia, H.; Wang, X.; Shalom, M. One-pot synthesis of nickel-modified carbon nitride layers toward efficient photoelectrochemical cells. *ACS Appl. Mater. Interfaces* **2017**, 9, 32667-32677.

Received: April 30, 2022
Accepted: May 27, 2022
Published online: June 10, 2022
Published: October 25, 2022

Xiaoxin Lv received her Ph.D. degree in 2016 from Institute of Functional Nano and Soft Materials Laboratory (FUNSOM), Soochow University. Currently, she is a lecturer in Automotive Engineering Research Institute, Jiangsu University. Her primary research interests focus on the design of advanced nanomaterials for photoelectrochemical water splitting and lithium-ion batteries.

Guoqing Li received his B.S. degree in Applied Chemistry from Henan Polytechnic University in 2020. Currently, he is a graduate student in Energy Research Institute in Jiangsu University. His research interests focus on photo/electrocatalysis water splitting.

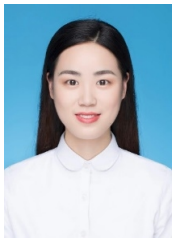

Gaoteng Zhang received her B.S. degree in Materials and Energy from Southwest University in 2020. Currently, she is a graduate student in Institute of Functional Nano & Soft Materials (FUNSOM) in Soochow University. Her research interests focus on hematite-based photoelectrochemical water splitting.

Kun Feng received his Ph.D. degree in 2020 from Soochow University. Currently, he performs postdoctoral research at the Institute of Functional Nano & Soft Materials (FUNSOM) at Soochow University. His research interests focus on the development of nano-scaled functional materials for electrocatalysis with the investigation of synchrotron radiation techniques.

Jiujun Deng is currently a professor of Institute for Energy Research, Jiangsu University. He received his Ph.D. from the Institute of Functional Nano & Soft Materials (FUNSOM) at Soochow University in 2016. After Ph.D., he worked as a postdoctoral fellow at Institut National de la Recherche Scientifique (INRS), Canada. His research interests focus on the design and synthesis of nanostructured functional materials for energy conversion and storage systems.

Jun Zhong is a full professor at the Institute of Functional Nano & Soft Materials (FUNSOM) at Soochow University. He received his B.E. degree from Tsinghua University in 2002, and his Ph.D. degree in 2007 from the Institute of High Energy Physics, CAS. He was a research scholar in 2006-2007 at ALS, Lawrence Berkeley National Laboratory. He became a research scientist in 2008 at the Institute of High Energy Physics and joined Soochow University in 2010. His research interests focus on the investigation of energy-related nanomaterials with synchrotron radiation techniques.

DOI: 10.14102/j.cnki.0254-5861.2022-0099